
When Pre-trained Visual Representations Fall Short: Limitations in Visuo-Motor Robot Learning

Nikolaos Tsagkas¹ Andreas Sochopoulos¹ Duolikun Danier¹ Chris Xiaoxuan Lu^{2†} Oisin Mac Aodha^{1†}

Abstract

The integration of pre-trained visual representations (PVRs) into visuo-motor robot learning has emerged as a promising alternative to training visual encoders from scratch. However, PVRs face critical challenges in the context of policy learning, including temporal entanglement and an inability to generalise even in the presence of minor scene perturbations. These limitations hinder performance in tasks requiring temporal awareness and robustness to scene changes. This work identifies these shortcomings and proposes solutions to address them. First, we augment PVR features with temporal perception and a sense of task completion, effectively disentangling them in time. Second, we introduce a module that learns to selectively attend to task-relevant local features, enhancing robustness when evaluated on out-of-distribution scenes. Our experiments demonstrate significant performance improvements, particularly in PVRs trained with masking objectives, and validate the effectiveness of our enhancements in addressing PVR-specific limitations. Project page: tsagkas.github.io/pvrobo

1. Introduction

Performing robust and accurate robotic manipulation from visual inputs necessitates informative and stable visual representations. The traditional paradigm for training visuo-motor policies has involved learning visual encoders from scratch alongside policy models (Levine et al., 2016). Recently, however, the adoption of pre-trained visual representations (PVRs), *i.e.*, computer vision models trained on large and diverse visual datasets, has emerged as a com-

promising alternative, moving away from the tabula-rasa approach (Parisi et al., 2022). This shift is driven by three key factors: the state-of-the-art performance of PVRs in computer vision tasks, their impressive generalisation capabilities derived from training on vast datasets, and the absence of robust robot-specific foundation models capable of addressing challenges unique to robotics, such as handling diverse embodiments.

Despite the promising results of PVRs in downstream robotic applications, including affordance-based manipulation (Li et al., 2024), semantically precise tasks (Tsagkas et al., 2024), and language-guided approaches (Shen et al., 2023), their integration into visuo-motor policy learning for even basic pick-and-place tasks remains an open challenge. Crucially, training visual encoders from-scratch or fine-tuning them with in-domain data still leads to competitive performance compared to using raw PVR features or even adapted PVRs (Sharma et al., 2023; Hansen et al., 2023). Furthermore, no single PVR, or set of characteristics, has consistently delivered optimal performance across diverse tasks and environments (Majumdar et al., 2023; Hu et al., 2023). Notably, their generalisation capabilities remain underutilised, as small scene variations can destabilise policy models (Caron et al., 2021; Xie et al., 2024), *c.f.* Fig. 3. This limitation has reignited interest in training models from scratch with augmented datasets (Hansen et al., 2023), a strategy that is prohibitively expensive for many real-world applications.

We identify critical shortcomings in the current use of PVRs for visuo-motor policy learning, rooted in the inherent nature of PVR features. First, we observe that these features are temporally entangled, primarily because widely used PVRs are designed as time-invariant models. Additionally, imitation learning datasets often consist of frame sequences where only minor changes occur in the pixel domain between adjacent timesteps. As a result, the extracted features from these frames remain highly similar, even at transition points where the corresponding actions may differ significantly. This discrepancy forces policy models to map nearly identical inputs to divergent outputs, introducing a problematic one-to-many mapping that violates the Markov property (see Fig. 1). Second, policy networks tend to overfit to

¹School of Informatics, University of Edinburgh, UK
²Department of Computer Science, University College London, UK. Correspondence to: Nikolaos Tsagkas <n.tsagkas@ed.ac.uk>.

Work under review. †indicates equal senior authorship.

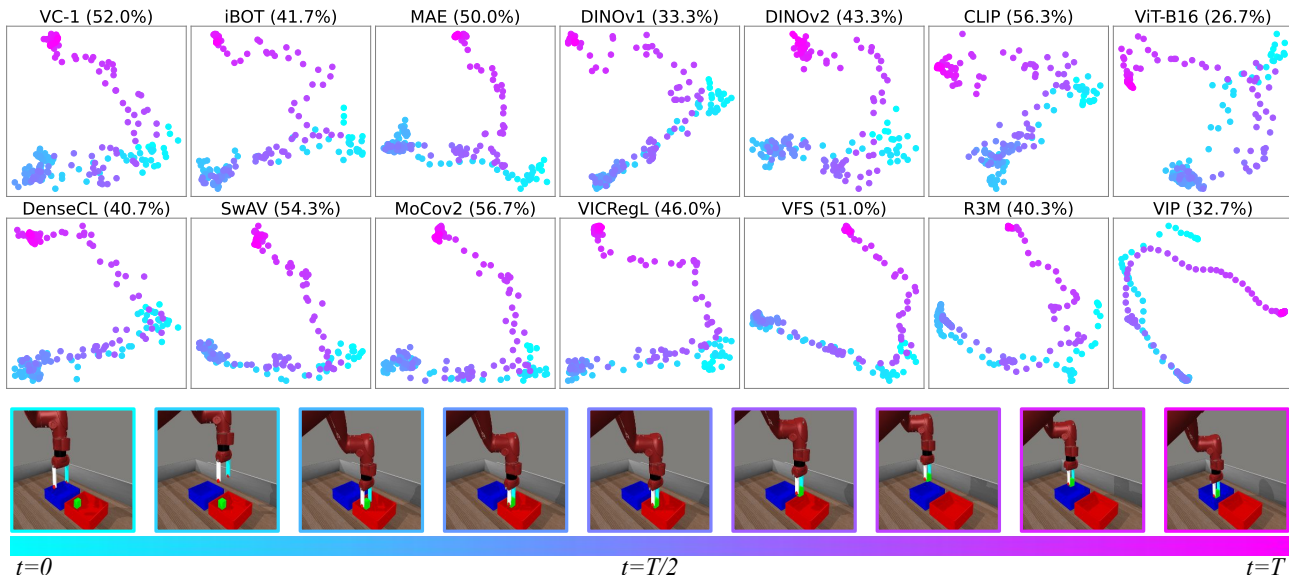


Figure 1. PCA of features from an expert demonstration in Bin Picking across PVRs (Top row: ViT models; Bottom row: ResNet models). Frame colours align with trajectory stages, suggesting feature entanglement during the gripper descent and ascent, and during the gripper stop phase. Our disentangling method improves success by 16.4% on the Bin Picking task, up from <50%.

features corresponding to dominant but irrelevant static visual cues (e.g., background elements), making them overly sensitive to minor scene perturbations. These seemingly small prediction errors accumulate over time, leading to substantial performance degradation.

We identify these inherent characteristics of PVRs as key factors hindering visuo-motor policy learning and argue that these issues should be addressed at the feature level. Attempting to resolve the temporal entanglement problem within the policy network would limit the flexibility of PVRs in general policy architectures. For example, an LSTM policy network could be a good candidate for that (Hausknecht & Stone, 2015), but would prevent us from conditioning other SoTA approaches, e.g., diffusion policies (Chi et al., 2023). Similarly, augmenting the dataset for improving the policy’s robustness (Hansen et al., 2023) would be prohibitive for real-world robot applications, as it would require a great number of man-hours and the fine-tuning of PVR weights could affect the rich encoded knowledge.

In summary, we make the following contributions:

- 1. Identifying PVR limitations:** We identify key characteristics of PVRs that hinder effective visuo-motor robot learning. Specifically, we show that they fail to encode the temporal cues and scene agnostic fine-scale visual features needed for precise manipulation tasks.
- 2. Temporal disentanglement:** We enhance PVR features by incorporating temporal awareness and task-completion perception, without altering the policy model architecture, yielding a statistically significant improvement in downstream task performance.
- 3. Targeted visual features:** We introduce a module

that learns to directly attend to task-relevant visual cues while ignoring scene distractors. Our approach does not require dataset augmentation or re-training but instead more effectively utilises existing PVR features, particularly benefiting masked image modelling (MIM) trained PVRs.

2. Related Work

2.1. PVRs in Visuo-motor Policy Learning

In (Parisi et al., 2022), frozen PVRs were evaluated across simulated environments, outperforming models trained from scratch. Similarly, (Hu et al., 2023) showed that the utility of PVRs depends on the policy training paradigm, with behaviour cloning and inverse reinforcement learning yielding robust results, while reinforcement learning exhibited higher variability. Furthermore, (Silwal et al., 2024) provided evidence that simulation experiments (e.g., Metaworld (Yu et al., 2020) benchmark) are indicative of real world performance for PVR-based trained policies.

The dataset(s) used for pre-training plays a pivotal role in PVRs. While it was hypothesised that pre-training with video data featuring egocentric human-object interaction would be highly effective for learning features suitable for robot learning (due to their emphasis on object manipulation), research indicates that the diversity of images within the dataset is a more critical factor in successful robot learning (Dasari et al., 2023; Majumdar et al., 2023). Indeed, PVRs pre-trained on static datasets such as ImageNet (Ridnik et al., 2021) have demonstrated competitive performance, underscoring the importance of dataset vari-

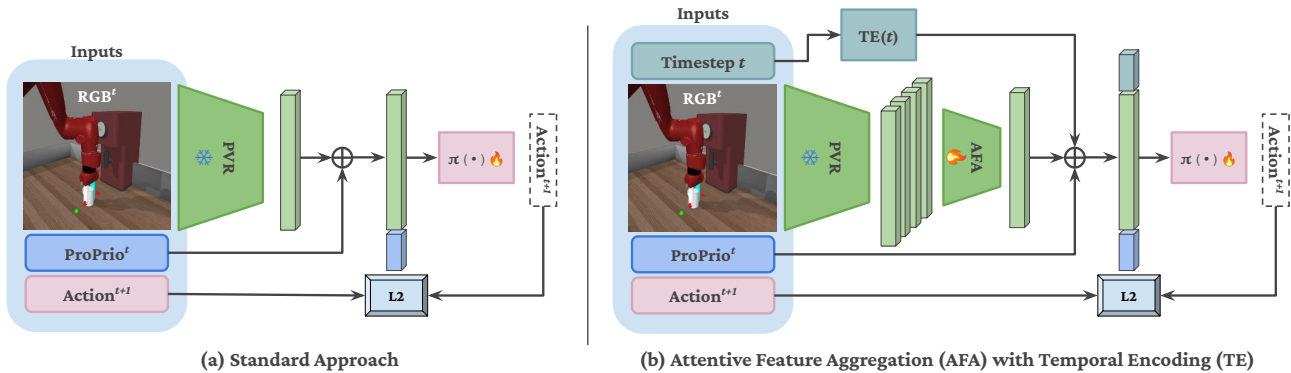


Figure 2. Standard PVR-based visuo-motor policy learning via behaviour cloning (a) and our approach (b), which integrates *Temporal Encoding (TE)* for temporal features (Section 3.2) and *Attentive Feature Aggregation (AFA)* for selective local feature attention (Section 3.3).

ability over modality.

PVRs are favoured for their generalisation capabilities in vision tasks, but out-of-distribution generalisation remains challenging in policy deployment. (Xie et al., 2024) analysed the impact of various perturbations on PVR-based policy generalisation, while (Burns et al., 2024) identified correlations between generalisation performance and inherent model traits, such as ViTs’ segmentation ability. Conversely, (Hansen et al., 2023) found that learning from scratch with data augmentation can yield competitive results, while (Lin et al., 2024) found that adapters (Houlsby et al., 2019) can improve policy generalisation when training with diverse object instances. We focus on developing methods that achieve robustness to scene changes without relying on dataset augmentation, which can be prohibitively expensive in real-world robotics applications. Particularly, our goal is to understand the reasons PVR-based policies struggle to generalise well and argue that there is more to be achieved with untouched frozen PVRs and that their full potential in visuo-motor policy learning is yet to be revealed.

2.2. Time-informed Policy Training

In PVR-based visuo-motor policy learning, the incorporation of temporal information remains underexplored. Augmentation with temporal perception can happen either at feature level or during training time.

Feature Augmentation. While early fusion methods, such as stacking multiple frames before encoding (Karpathy et al., 2014), are common in training visual encoders from scratch, late fusion-processing frames individually and stacking their representations (Vaswani et al., 2017) has shown superior performance with fewer encoder parameters. Recent work (Shang et al., 2021) highlights that naive feature concatenation in latent space is insufficient; instead, approaches like FLARE (Shang et al., 2021) incorporate sequential embeddings and their differences, inspired by optical flow techniques. Nevertheless, concatenating sequential embed-

dings as input to policy networks has become standard in visuo-motor policy learning (Parisi et al., 2022) and state-of-the-art generative policies (Chi et al., 2023). However, a gap remains in leveraging PVR features, which are primarily designed for vision tasks, within this temporal framework.

Loss Function Augmentation. A major limitation of many PVRs is their inherent lack of temporal perception, as most are pre-trained on static 2D image datasets. Temporal perception can be added by employing loss functions that enforce temporal consistency during training (e.g., R3M (Nair et al., 2022) and VIP (Ma et al., 2023b)), when training with video data. However, there is no clear consensus on the superiority of this approach compared to alternatives like MIM (e.g., MVP (Xiao et al., 2022; Hu et al., 2023) and VC-1 (Majumdar et al., 2023)). This disparity suggests that existing temporal modelling strategies may be insufficient in isolation.

In subsequent experiments, we evaluate PVRs trained with temporal information and demonstrate that methods trained with a time-agnostic paradigm achieve comparable performance. We hypothesise that this limitation arises from a lack of task-completion perception, which we address by incorporating positional encoding—a fundamental mechanism in many machine learning approaches. This straightforward operation has been instrumental in the success of Transformers (Vaswani et al., 2017), implicit spatial representations (Mildenhall et al., 2020), and diffusion models (Ho et al., 2020).

2.3. Task-Relevant Feature Extraction

Downstream vision tasks often make use of the output features of PVRs. However, these features typically encode a broad range of scene information, much of which may be irrelevant to the specific task. To address this challenge, attentive probing (Chen et al., 2024; Danier et al., 2024; Bardes et al., 2024) has emerged as a popular evaluation technique, leveraging local tokens. This approach leverages

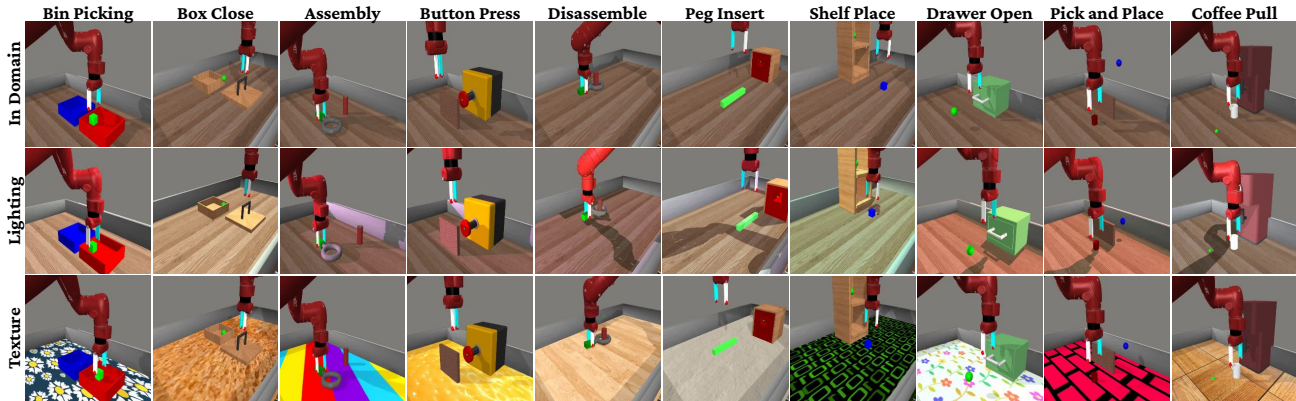


Figure 3. Visualisation of the 10 tasks used for evaluation. The first row illustrates representative scenes for all tasks, as seen in the frames from the expert demonstrations (in-domain). The second row shows how the scenes are modified by randomly altering the brightness, orientation and position of the light source. Similarly, the third row presents changes to the tabletop texture.

a cross-attention layer with a trainable query token, treating the local features from PVRs as a sequence of key-value pairs. Unlike traditional evaluation methods such as linear probing, attentive probing has shown significantly different vision evaluation outcomes, particularly with PVRs trained using MIM approaches (e.g., MAE (He et al., 2022)), where features, such as the CLS token, often include irrelevant information. Similarly, in robot learning, task-relevant signals like joint angles may correspond to particular image regions, with unrelated cues acting as distractions. By prioritizing task-relevant signals, we show that attentive probing enhances task performance, especially in out-of-distribution scenarios.

3. Methodology

In this section, we present our approaches to enhance the deployment of PVRs in visuo-motor policy learning. First, we introduce the general behaviour cloning framework commonly employed in this domain (Section 3.1). Then, we describe a method to enrich features with temporal information, aimed at mitigating issues of temporal ambiguity (Section 3.2). Finally, we introduce our approach to selectively attend to task-relevant components of PVR features, improving their utility for robot learning tasks (Section 3.3).

3.1. Preliminaries

Imitation Learning via Behaviour Cloning. We consider an expert policy $\pi^* : \mathcal{P} \times \mathcal{O} \rightarrow \mathcal{A}$, which maps the current proprioceptive observation $p \in \mathcal{P}$ of a robot manipulator and a visual observation $o \in \mathcal{O}$ to a corresponding robot action $a \in \mathcal{A}$. This expert policy is used to generate a dataset of expert demonstrations, D_{exp} , consisting of N trajectories $\mathcal{T}^e = \{(p_t^i, o_t^i, a_t^i)_{t=0}^T\}_{i=1}^N$, where each trajectory captures the sequence of observations, and actions recorded over T timesteps while solving a task.

The goal of behavioural cloning is to learn a policy π_θ , parameterised by θ , that closely imitates the expert policy by minimizing the discrepancy between its actions and the expert’s actions. This is formulated as a supervised learning problem, where the loss function measures this discrepancy across the dataset of demonstrations:

$$\mathbb{E}_{(p_t^i, o_t^i, a_t^i) \sim \mathcal{T}^e} \|a_t^i - \pi_\theta(f_{\text{PVR}}(o_t^i), p_t^i)\|_2^2, \quad (1)$$

where f_{PVR} represents a PVR that acts as a feature extraction function used to process visual observations o_t^i .

In robot learning, the decision-making process is commonly assumed to satisfy the Markov property. This assumption implies that the current observation $x_t = (p_t, o_t)$ encapsulates all the information necessary for predicting the subsequent state, i.e., $P(x_{t+1}|x_t) = P(x_{t+1}|x_t, x_{t-1}, \dots, x_0)$. Consequently, tasks are modelled as sequences of decisions, where each action depends solely on the current state, facilitating the application of behaviour cloning under this framework.

3.2. Temporal Disentanglement

We find that the assumption of Markovian decision-making in policies based on features extracted from frozen PVRs is frequently invalid. This arises because, at each timestep, the available information may be insufficient for the policy to confidently map the current observation to the appropriate action.

Consider the example presented in Fig. 1, where PVR-features of the same pick-and-place trajectory are projected with PCA into 2D. Regardless of the PVR utilised, the extracted features seem to suffer from temporal entanglement. First, features extracted from the frames where the robot has stopped to pick up the box form a tight cluster, since the only change is the movement of the gripper fingers, which corresponds to a very small percentage of pixels. Second, as the gripper moves down and subsequently ascends, the

primary visual change is the cube’s vertical displacement relative to the table. Consequently, the visual features extracted from the descent and ascent frames may differ only marginally, and only in dimensions affected by the small pixel region of the cube.

Fig. 1 also hints that including proprioceptive data in the policy input is not necessarily adequate to resolve these ambiguities. This is either because the high-dimensionality of visual features often dominates the lower-dimensional proprioceptive input, or because the robot may follow nearly identical trajectories while performing a task, further compounding the difficulty of disentangling visually similar states. At the same time, prior methods, where features from successive images were concatenated alone (Parisi et al., 2022) or along with their differences (Shang et al., 2021), have been effective to some extent. However, if frame-to-frame appearance differences are minimal, the resulting features can be very similar, and thus their differences predominantly contain near-zero values.

Training a policy network to map (p_t, o_t) to a_t becomes difficult under these conditions. When multiple observations are nearly indistinguishable, the mapping violates the functional requirement that each input must map to exactly one output. To address these challenges, we propose a simple yet effective method to augment each observation with a temporal component by encoding the timestep index of each frame as a high-dimensional vector, using Eq. 2. This augmentation can temporally disentangle similar (p_t, o_t) pairs, introducing a task progression signal into the robot state, which we argue can substantially enhance policy performance.

$$\gamma(t) = \left(\sin\left(\frac{2^0 \pi t}{s^0}\right), \cos\left(\frac{2^0 \pi t}{s^0}\right), \dots, \sin\left(\frac{2^{T-1} \pi t}{s^{T-1}}\right), \cos\left(\frac{2^{T-1} \pi t}{s^{T-1}}\right) \right) \quad (2)$$

Eq. 2 encodes the timestep t into a high-dimensional vector $\gamma(t)$ using alternating sine and cosine functions at exponentially increasing frequencies 2^k . The lower-frequency terms capture coarse temporal trends, while the higher-frequency terms provide finer temporal resolution, enabling the policy to distinguish between temporally similar states.

3.3. Attending to Policy Related Features

We posit that training policies using the global features of PVRs (*i.e.*, CLS token for ViTs or average channel feature for ResNets) leads to overfitting to scene conditions that are irrelevant to the task at hand. The output features of these representations often capture visual characteristics of the scene that may be irrelevant to the policy (*e.g.*, the texture

of a tabletop). Processing such extraneous information not only dilutes the policy network’s focus but also leads to overfitting to specific scene conditions.

This observation aligns with recent work on vision model evaluation (Chen et al., 2024), which argues that only specific image regions carry the necessary information for solving a task. Building on this insight, we hypothesise that incorporating local information is particularly effective in the context of robot learning, echoing findings in PVR distillation research (Shang et al., 2024), though this area remains empirically underexplored.

Recognizing the importance of local information is only part of the solution; a data-driven mechanism is also required to filter irrelevant details, such as background patches, and prioritise task-relevant information. To this end, we adopt the *attentive probing* methodology to implement *Attentive Feature Aggregation* (AFA). Specifically, we append a cross-attention layer to the frozen PVR, modified to include a trainable query token that interacts with the sequence of local tokens produced by the model. These tokens correspond to the per-patch embeddings for ViTs and the channel embeddings for ResNets, both from the final layer.

Following Eq. 3, the query token q computes dot products with the feature sequence, with length equal to #patches and dimension d_k , organized as a matrix F . These dot products are passed through a softmax function to assign weights to the contributions of each local token to the final embedding. Also, our module consists of multiple heads, so that specific dimension groups that might be irrelevant to the policy can be filtered out. Gradients are allowed to flow through the cross-attention layer, updating the parameters of q as well as the key and value projection matrices, W_K and W_V .

$$\text{Attention}(q, F) = \text{softmax}\left(\frac{q \cdot (F \cdot W_K)^T}{\sqrt{d_k}}\right) F \cdot W_V \quad (3)$$

4. Experiments

4.1. Setup

Environment. We conduct our experiments in the widely used MetaWorld simulation environment (Yu et al., 2020), which is built on the MuJoCo (Todorov et al., 2012) physics engine. From this benchmark, we select the ten tasks visualised in Fig. 3 and generate 25 expert demonstrations with 175 rollout steps for each using the provided heuristic policies. The primary criterion for task selection is to maintain a balanced representation of easy, medium, and hard tasks, as identified in prior work on PVR-based visuo-motor control (Mete et al., 2024; Hu et al., 2023), as well as in our empirical results.

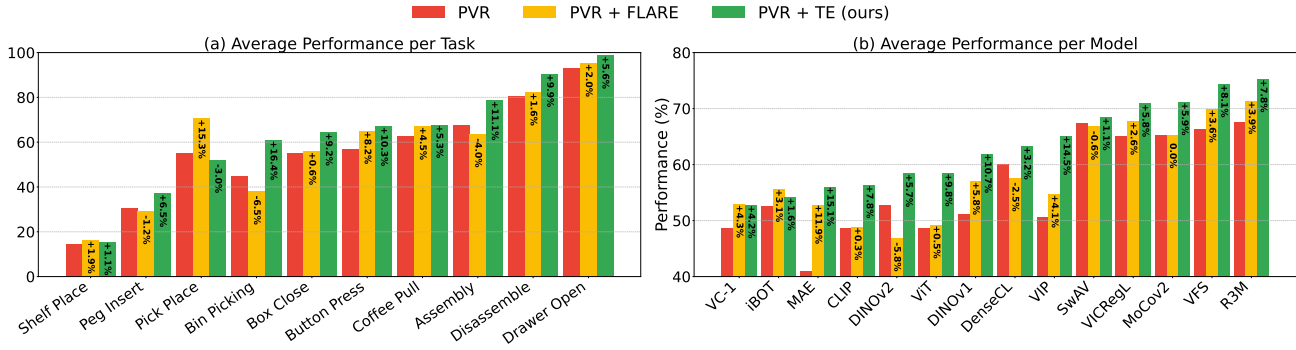


Figure 4. Comparison of Temporal Encoding (TE) against FLARE (Shang et al., 2021) and using no temporal augmentation on PVR features. Results (sorted by TE) show (a) per-task performance and (b) per-model performance. FLARE and TE bars indicate gains over no temporal information.

PVRs. To validate our hypotheses, we deploy seven Residual Networks (ResNets) (He et al., 2016) and seven Vision Transformers (ViT) (Dosovitskiy et al., 2021), as summarised in Tab. A1 in the Appendix. Our selection includes the most popular PVRs utilised in robot learning applications that have led to SoTA performance. We also focused on ensuring diversity in training strategies, datasets, and the balance between local and global perception. Despite these variations, we maintain a consistent backbone architecture of ResNet-50 or ViT-B/16, with the exception of DINOv2, which employs a smaller patch size of 14. Also, for DINOv2 we discard overlapping patches, to ensure fairness in the comparison of PVRs. The models tested include powerful representations from vision-specific approaches (e.g., DINO), vision-language models (e.g., CLIP), and robot-learning-focused models (e.g., R3M).

Policy training. For all policy training, we train the policy network five times, using five different seeds, keeping the PVR frozen, and report the interquartile mean (IQM) success rate. As is common practice in similar work (Parisi et al., 2022; Nair et al., 2022; Hu et al., 2023), our policy head consists of a small number of MLP layers (four in our case), separated by ReLUs, and outputs the predicted action. We train with mini-batches of 128 samples for 80,000 steps.

4.2. Temporal Encoding

We evaluate the performance of a policy network trained for each PVR under three conditions: without any temporal component, using the three most recent past observations and their latent differences (i.e., FLARE (Shang et al., 2021)), and with our proposed Temporal Encoding (TE) method. We select the dimensionality of TE to be 64 and the scale parameter 100, after tuning these hyperparameters in a subset of tasks and PVRs (see Appendix C.3).

Fig. 4 illustrates (a) the average performance per task for each of the three approaches and (b) the average performance per model. Statistical analysis (paired t-tests,

Wilcoxon tests-results in Appendix C.2) confirms TE’s gains over FLARE and no augmentation are significant. While VC-1 and iBOT achieve slightly higher average scores with FLARE, all other PVRs benefit significantly from temporal augmentation, even when compared to FLARE-augmented results. Similarly, apart from the “Pick and Place” and “Shelf Place” tasks, TE significantly enhances the average task performance. We attribute TE’s superiority over FLARE to the fact that FLARE’s method of stacking sequential latent embeddings, along with their differences, results in embeddings that are nearly identical due to the high similarity of features extracted from consecutive observations. Consequently, the differences between these embeddings are often near-zero vectors, limiting FLARE’s ability to effectively leverage temporal information. Table A2 provides a detailed summary of the performance of each model-task pair.

An intriguing observation is that PVRs pre-trained with a temporal component in their objective function also benefit considerably from TE. For instance, R3M employs time-contrastive learning (Sermanet et al., 2017) to enforce similarity between representations of temporally adjacent frames-experience substantial gains from TE. Notably, VIP achieves an average performance boost of approximately 15 percentage points, making it one of the most positively impacted models. This finding suggests a potential reconsideration of how temporal perception is integrated into features designed for robot learning. It raises the possibility that existing approaches may not fully exploit the temporal structure necessary for optimal performance.

4.3. Attentive Feature Aggregation

We utilise a cross-attention layer and use 12 attention heads for features extracted from ViTs and 32 for features from ResNets. This configuration ensures that we process 64-dimensional feature chunks in both cases, maintaining fairness between the two backbone architectures. Consistent

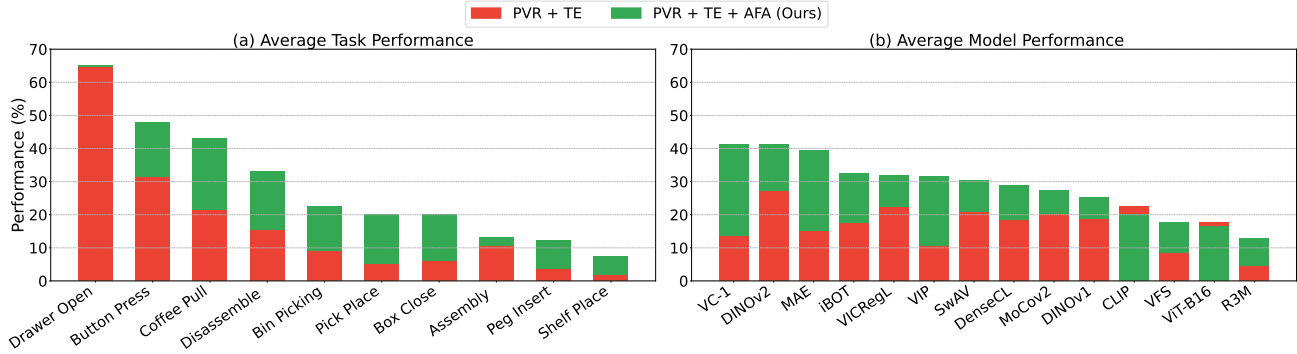


Figure 5. Robustness evaluation of policies trained with PVR-extracted features temporally augmented with TE, and with features processed using AFA and temporally augmented with TE. The evaluation is conducted under perturbed lighting conditions and tabletop texture changes. Subplot (a) shows the average performance per task, while subplot (b) shows the average performance per model.

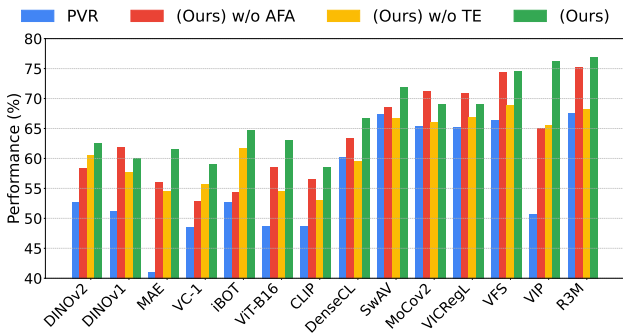


Figure 6. Ablation study on our approach (*i.e.*, PVR+TE+AFA). Results are reported on in-domain scenes.

with standard attentive probing methodologies (Chen et al., 2024; Danier et al., 2024), we employ a cosine learning rate scheduler with a warm-up phase. In all experiments, TE is applied to augment features with a temporal component. Specifically, for AFA, the temporal feature is concatenated with the output of the cross-attention module. We validate our full model’s significance via an ablation study, presented in Fig. 6, that evaluates the contributions of TE and AFA in our approach, comparing it against training the policy network solely with PVR-extracted features.

We hypothesise that AFA learns to attend only to scene areas that are important to the task, disregarding features irrelevant to the policy. To properly evaluate this component, we do not limit our evaluation to in-domain scenes but also with environments recreated with scene perturbations, leaving the training dataset distribution unchanged. These perturbations include two modifications, details of which are included in Appendix D.2. First, tabletop texture changes, randomly selected from 30 distinct textures, some of which feature vibrant patterns that act as strong distractors. These changes affect a significant area of the frame. Second, variations in lighting conditions, including adjustments to the orientation, position, and brightness of

the light source. These modifications influence the entire frame, including the robot and the object it manipulates.

We summarize the performance of policies trained directly with PVR features and those trained with features aggregated using AFA in Fig. 5, averaged across tasks and models on perturbed scenes. We also provide in Fig. A4 a concise summary of the performance of each task and model pair on in-domain scenes and on perturbed scenes (per perturbation category).

From these results, several trends emerge. AFA consistently improves the robustness of policies across all tasks, often yielding significant gains, with some tasks showing up to a threefold improvement. The only exception is the “Drawer Open” task, which sees little benefit from AFA. This is likely due to its inherent simplicity, as the task involves manipulating a large object without requiring control of the gripper fingers, which remain open throughout the demonstrations. Consequently, attending to local observations has limited impact.

Additionally, most models exhibit improved out-of-distribution performance with AFA, except for CLIP and ViT-B/16. This is reasonable, as these models are trained with objectives that emphasise global frame perception, unlike other models that incorporate supervision at the patch level. Notably, MIM-trained PVRs benefit the most from AFA, reflecting the alignment between AFA’s design, which is inspired by attentive probing, and the training principles of MIM-based models. These findings highlight AFA’s ability to enhance policy performance, particularly in challenging out-of-distribution scenarios, and underscore its compatibility with models that leverage local feature representations.

The average in-domain performance remains nearly unchanged, with a slight increase from 63.1% to 66.4% when using AFA. The minor performance boost observed with AFA in in-domain scenarios, especially when compared to its substantial improvements in perturbed scenes, sug-

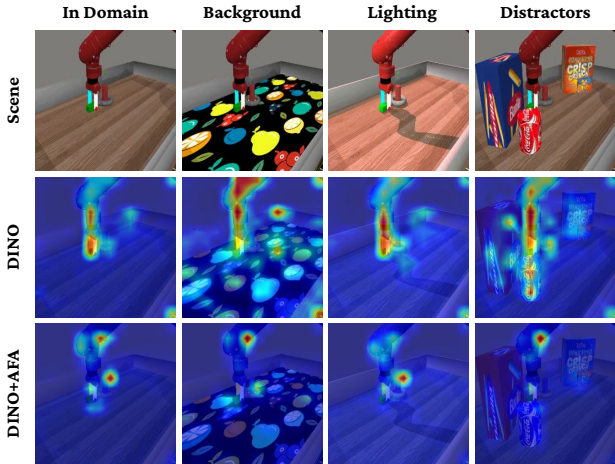


Figure 7. Comparison of attention heatmaps between the DINO and DINO+AFA (ours). The latter learns to focus on task-relevant regions and ignores scene changes (e.g., distractor objects). Visualisations from more PVRs are included in Fig. A7.

gests that AFA does not learn a new latent space for the PVR that is more suited to the task. Instead, it appears to refine the use of the existing latent space by learning to effectively leverage relevant information while discarding elements that are irrelevant to the policy. This distinction underscores AFA’s role as a mechanism for better utilisation of pre-trained features rather than redefining or adapting the underlying feature space.

5. Discussion

We explored how to effectively utilise PVRs for visuo-motor policy learning, identifying the issues of feature temporal entanglement and lack of robustness in scene visual changes. Furthermore, we proposed two approaches to address these limitations leading to a significant performance increase. Below we provide a set of questions with answers that we believe further highlight the contributions of our work.

Q:Does TE help because expert demos are time synced?

A: Even though the expert demos are generated by a heuristic policy, in Fig. A3 we show that they are actually not synchronised and the only common factor is that the task is always completed by $T=175$ steps.

Q:Does AFA’s robustness stem from the additional trainable parameters?

A: AFA introduces approximately 1.5M additional parameters to a policy model that originally has around 0.5M parameters. To determine whether the observed performance improvement is simply due to the increased model capacity, we train a policy network using raw PVR features but design a deeper policy network to match AFA’s parameter count. The results, shown for two tasks in Fig. A6, suggest otherwise. This indicates that the performance gains arise

from AFA’s ability to effectively attend to local information, as is suggested by Fig. 7.

Q:Does the simulation’s lack of visual realism affect the perception of PVRs?

A: Empirical evidence has shown that simulations serve as a reliable proxy for PVR-based visuo-motor policy learning, particularly in environments like MetaWorld (Silwal et al., 2024). To further validate this, we replicate the visualization in Fig. 1 for an expert demonstration in two real-world tasks. The results in Fig. A2 and Fig. A1, reveal that the same feature-related issues persist, underscoring the relevance of our findings across both simulated and real-world settings.

Q:Why is there still a significant performance gap under scene perturbations?

A: We posit that the remaining performance gap largely stems from inherent limitations of behaviour cloning. Its supervised nature makes the policy network vulnerable to compounding errors. Despite improved feature attention, the models tend to overfit to specific visual settings, making it sensitive to domain shifts that progressively push the policy out-of-distribution.

Q:Can we get even better policy performance?

A: Behaviour cloning performance is largely dependent on how well the expert policy π^* is sampled. Increasing the number of demonstrations or utilising techniques like DAGger (Ross et al., 2011) could help mitigate this issue.

Limitations. We conducted extensive experiments, evaluating multiple PVRs and training policies across different seeds and representative tasks. However, our work has certain limitations. First, while MetaWorld serves as a reliable and widely used proxy for robot learning experiments, we have not tested our methods on a real robot. Evaluating their effectiveness in real-world scenarios remains an important direction for future research. Second, in line with common practice, we use a simple MLP policy network to ensure our approach targets the feature space and remains agnostic to policy architecture. However, it would be valuable to explore how our methods impact state-of-the-art policy models, such as diffusion-based approaches, which are known to struggle when conditioned on PVRs (Chi et al., 2023). Future work should address these limitations by assessing our approach with alternative policy architectures trained end-to-end with visual encoders.

6. Conclusion

The use of PVRs for visuo-motor policy learning is still in its early stages, and we believe our work paves the way for further exploration of key challenges. Our insights contribute to the development of PVR models specifically designed for robot learning, ultimately leading to a generalist robotic system powered by large-scale vision foundation models.

Impact Statement

This paper presents work whose goal is to advance the field of Machine Learning and Robotics. There are many potential societal consequences of our work, none which we feel must be specifically highlighted here.

References

- Bardes, A., Ponce, J., and LeCun, Y. Vicregl: Self-supervised learning of local visual features. *Advances in Neural Information Processing Systems (NeurIPS)*, 2022.
- Bardes, A., Garrido, Q., Ponce, J., Rabbat, M., LeCun, Y., Assran, M., and Ballas, N. Revisiting feature prediction for learning visual representations from video. *arXiv:2404.08471*, 2024.
- Burns, K., Witzel, Z., Hamid, J. I., Yu, T., Finn, C., and Hausman, K. What makes pre-trained visual representations successful for robust manipulation? In *Conference on Robot Learning (CoRL)*, 2024.
- Caron, M., Misra, I., Mairal, J., Goyal, P., Bojanowski, P., and Joulin, A. Unsupervised learning of visual features by contrasting cluster assignments. *Advances in Neural Information Processing Systems (NeurIPS)*, 2020.
- Caron, M., Touvron, H., Misra, I., Jégou, H., Mairal, J., Bojanowski, P., and Joulin, A. Emerging properties in self-supervised vision transformers. In *International Conference on Computer Vision (ICCV)*, 2021.
- Chen, X., Fan, H., Girshick, R., and He, K. Improved baselines with momentum contrastive learning. *arXiv preprint arXiv:2003.04297*, 2020.
- Chen, X., Ding, M., Wang, X., Xin, Y., Mo, S., Wang, Y., Han, S., Luo, P., Zeng, G., and Wang, J. Context autoencoder for self-supervised representation learning. *International Journal of Computer Vision (IJCV)*, 132(1): 208–223, 2024.
- Chi, C., Feng, S., Du, Y., Xu, Z., Cousineau, E., Burchfiel, B., and Song, S. Diffusion policy: Visuomotor policy learning via action diffusion. In *Robotics: Science and Systems (RSS)*, 2023.
- Danier, D., Aygün, M., Li, C., Bilen, H., and Mac Aodha, O. DepthCues: Evaluating Monocular Depth Perception in Large Vision Models. *arXiv:2411.17385*, 2024.
- Dasari, S., Srirama, M. K., Jain, U., and Gupta, A. An unbiased look at datasets for visuo-motor pre-training. In *Conference on Robot Learning (CoRL)*, 2023.
- Dosovitskiy, A., Beyer, L., Kolesnikov, A., Weissenborn, D., Zhai, X., Unterthiner, T., Dehghani, M., Minderer, M., Heigold, G., Gelly, S., Uszkoreit, J., and Houlsby, N. An image is worth 16x16 words: Transformers for image recognition at scale. In *International Conference on Learning Representations (ICLR)*, 2021.
- Florence, P., Manuelli, L., and Tedrake, R. Self-supervised correspondence in visuomotor policy learning. In *Robotics and Automation Letters (RA-L)*, 2019.
- Florence, P., Lynch, C., Zeng, A., Ramirez, O., Wahid, A., Downs, L., Wong, A., Lee, J., Mordatch, I., and Tompson, J. Implicit behavioral cloning. *Conference on Robot Learning (CoRL)*, 2021.
- Florence, P. R., Manuelli, L., and Tedrake, R. Dense object nets: Learning dense visual object descriptors by and for robotic manipulation. In *Conference on Robot Learning (CoRL)*, 2018.
- Ganapathi, A., Sundaresan, P., Thananjeyan, B., Balakrishna, A., Seita, D., Grannen, J., Hwang, M., Hoque, R., Gonzalez, J. E., Jamali, N., et al. Learning dense visual correspondences in simulation to smooth and fold real fabrics. In *International Conference on Robotics and Automation (ICRA)*, 2021.
- Gupta, G., Yadav, K., Gal, Y., Batra, D., Kira, Z., Lu, C., and Rudner, T. G. Pre-trained text-to-image diffusion models are versatile representation learners for control. *arXiv preprint arXiv:2405.05852*, 2024.
- Hansen, N., Yuan, Z., Ze, Y., Mu, T., Rajeswaran, A., Su, H., Xu, H., and Wang, X. On pre-training for visuo-motor control: Revisiting a learning-from-scratch baseline. In *International Conference on Machine Learning (ICML)*, 2023.
- Hausknecht, M. J. and Stone, P. Deep recurrent q-learning for partially observable mdps. In *Association for the Advancement of Artificial Intelligence (AAAI) Fall Symposium*, 2015.
- He, K., Zhang, X., Ren, S., and Sun, J. Deep residual learning for image recognition. In *Computer Vision and Pattern Recognition (CVPR)*, 2016.
- He, K., Chen, X., Xie, S., Li, Y., Doll’ar, P., and Girshick, R. B. Masked autoencoders are scalable vision learners. *Conference on Computer Vision and Pattern Recognition (CVPR)*, 2022.
- Ho, J., Jain, A., and Abbeel, P. Denoising diffusion probabilistic models. In *Advances in Neural Information Processing Systems (NeurIPS)*, 2020.
- Houlsby, N., Giurgiu, A., Jastrzebski, S., Morrone, B., De Laroussilhe, Q., Gesmundo, A., Attariyan, M., and Gelly, S. Parameter-efficient transfer learning for NLP. In

- International Conference on Machine Learning (ICML)*, 2019.
- Hu, Y., Wang, R., Li, L. E., and Gao, Y. For pre-trained vision models in motor control, not all policy learning methods are created equal. In *International Conference on Machine Learning (ICML)*, 2023.
- Karamcheti, S., Nair, S., Chen, A. S., Kollar, T., Finn, C., Sadigh, D., and Liang, P. Language-driven representation learning for robotics. In *Robotics: Science and Systems (RSS)*, 2023.
- Karpathy, A., Toderici, G., Shetty, S., Leung, T., Sukthankar, R., and Fei-Fei, L. Large-scale video classification with convolutional neural networks. In *Conference on Computer Vision and Pattern Recognition (CVPR)*, 2014.
- Levine, S., Finn, C., Darrell, T., and Abbeel, P. End-to-end training of deep visuomotor policies. *Journal of Machine Learning Research (JMLR)*, 17(39):1–40, 2016.
- Li, G., Tsagkas, N., Song, J., Mon-Williams, R., Vijayakumar, S., Shao, K., and Sevilla-Lara, L. Learning precise affordances from egocentric videos for robotic manipulation. *arXiv preprint arXiv:2408.10123*, 2024.
- Li, X., Liu, M., Zhang, H., Yu, C., Xu, J., Wu, H., Cheang, C., Jing, Y., Zhang, W., Liu, H., Li, H., and Kong, T. Vision-language foundation models as effective robot imitators. *arXiv preprint arXiv:2311.01378*, 2023.
- Lin, X., So, J., Mahalingam, S., Liu, F., and Abbeel, P. Spawnet: Learning generalizable visuomotor skills from pre-trained network. In *International Conference on Robotics and Automation (ICRA)*, 2024.
- Ma, Y. J., Kumar, V., Zhang, A., Bastani, O., and Jayaraman, D. Liv: language-image representations and rewards for robotic control. In *International Conference on Machine Learning (ICML)*, ICML, 2023a.
- Ma, Y. J., Sodhani, S., Jayaraman, D., Bastani, O., Kumar, V., and Zhang, A. VIP: Towards universal visual reward and representation via value-implicit pre-training. In *International Conference on Learning Representations (ICLR)*, 2023b.
- Majumdar, A., Yadav, K., Arnaud, S., Ma, J., Chen, C., Silwal, S., Jain, A., Berges, V.-P., Wu, T., Vakil, J., Abbeel, P., Malik, J., Batra, D., Lin, Y., Maksymets, O., Rajeswaran, A., and Meier, F. Where are we in the search for an artificial visual cortex for embodied intelligence? In *Advances in Neural Information Processing Systems (NeurIPS)*, 2023.
- Manuelli, L., Li, Y., Florence, P., and Tedrake, R. Keypoints into the future: Self-supervised correspondence in model-based reinforcement learning. In *Conference on Robot Learning (CoRL)*, 2021.
- Mete, A., Xue, H., Wilcox, A., Chen, Y., and Garg, A. Quest: Self-supervised skill abstractions for learning continuous control. In *Advances in Neural Information Processing Systems (NeurIPS)*, 2024.
- Mildenhall, B., Srinivasan, P. P., Tancik, M., Barron, J. T., Ramamoorthi, R., and Ng, R. Nerf: Representing scenes as neural radiance fields for view synthesis. In *European Conference on Computer Vision (ECCV)*, 2020.
- Nair, S., Rajeswaran, A., Kumar, V., Finn, C., and Gupta, A. R3m: A universal visual representation for robot manipulation. In *Conference on Robot Learning (CoRL)*, 2022.
- Oquab, M., Darcet, T., Moutakanni, T., Vo, H. V., Szafraniec, M., Khalidov, V., Fernandez, P., Haziza, D., Massa, F., El-Nouby, A., Howes, R., et al. Dinov2: Learning robust visual features without supervision. *Transactions on Machine Learning Research (TMLR)*, 2024.
- Parisi, S., Rajeswaran, A., Purushwalkam, S., and Gupta, A. The (un)surprising effectiveness of pre-trained vision models for control. In *International Conference on Machine Learning (ICML)*, 2022.
- Radford, A., Kim, J. W., Hallacy, C., Ramesh, A., Goh, G., Agarwal, S., Sastry, G., Askell, A., Mishkin, P., Clark, J., et al. Learning transferable visual models from natural language supervision. In *International Conference on Machine Learning (ICML)*, 2021.
- Ridnik, T., Ben-Baruch, E., Noy, A., and Zelnik-Manor, L. Imagenet-21k pretraining for the masses. In *Advances in Neural Information Processing Systems Track on Datasets and Benchmarks*, 2021.
- Ross, S., Gordon, G., and Bagnell, D. A reduction of imitation learning and structured prediction to no-regret online learning. In *International Conference on Artificial Intelligence and Statistics (AISTATS)*, 2011.
- Sermanet, P., Xu, K., and Levine, S. Unsupervised perceptual rewards for imitation learning. In *Robotics: Science and Systems (RSS)*, 2017.
- Shafiullah, N. M. M., Paxton, C., Pinto, L., Chintala, S., and Szlam, A. Clip-fields: Weakly supervised semantic fields for robotic memory. In *Robotics: Science and Systems (RSS)*, 2023.

- Shang, J., Schmeckpeper, K., May, B. B., Minniti, M. V., Kelestemur, T., Watkins, D., and Herlant, L. Theia: Distilling diverse vision foundation models for robot learning. In *Conference on Robot Learning (CoRL)*, 2024.
- Shang, W., Wang, X., Srinivas, A., Rajeswaran, A., Gao, Y., Abbeel, P., and Laskin, M. Reinforcement learning with latent flow. In *Advances in Neural Information Processing Systems (NeurIPS)*, 2021.
- Sharma, M., Fantacci, C., Zhou, Y., Koppula, S., Heess, N., Scholz, J., and Aytar, Y. Lossless adaptation of pretrained vision models for robotic manipulation. In *International Conference on Learning Representations (ICLR)*, 2023.
- Shen, W., Yang, G., Yu, A., Wong, J., Kaelbling, L. P., and Isola, P. Distilled feature fields enable few-shot language-guided manipulation. In *Conference on Robot Learning (CoRL)*, 2023.
- Silwal, S., Yadav, K., Wu, T., Vakil, J., Majumdar, A., Arnaud, S., Chen, C., Berges, V.-P., Batra, D., Rajeswaran, A., Kalakrishnan, M., Meier, F., and Maksymets, O. What do we learn from a large-scale study of pre-trained visual representations in sim and real environments? In *International Conference on Robotics and Automation (ICRA)*, 2024.
- Sochopoulos, A., Gienger, M., and Vijayakumar, S. Learning deep dynamical systems using stable neural odes. In *International Conference on Intelligent Robots and Systems (IROS)*, 2024.
- Sundaresan, P., Grannen, J., Thananjeyan, B., Balakrishna, A., Laskey, M., Stone, K., Gonzalez, J. E., and Goldberg, K. Learning rope manipulation policies using dense object descriptors trained on synthetic depth data. In *International Conference on Robotics and Automation (ICRA)*, 2020.
- Todorov, E., Erez, T., and Tassa, Y. Mujoco: A physics engine for model-based control. In *IEEE/RSJ International Conference on Intelligent Robots and Systems (IROS)*, 2012.
- Tsagkas, N., Mac Aodha, O., and Lu, C. X. VI-fields: Towards language-grounded neural implicit spatial representations. In *International Conference on Robotics and Automation Workshops (ICRA)*, 2023.
- Tsagkas, N., Rome, J., Ramamoorthy, S., Mac Aodha, O., and Lu, C. X. Click to grasp: Zero-shot precise manipulation via visual diffusion descriptors. In *International Conference on Intelligent Robots and Systems (IROS)*, 2024.
- Vaswani, A., Shazeer, N., Parmar, N., Uszkoreit, J., Jones, L., Gomez, A. N., Kaiser, L. u., and Polosukhin, I. Attention is all you need. In *Advances in Neural Information Processing Systems (NeurIPS)*, 2017.
- Wang, X., Zhang, R., Shen, C., Kong, T., and Li, L. Dense contrastive learning for self-supervised visual pre-training. In *Conference on Computer Vision and Pattern Recognition (CVPR)*, 2021.
- Wang, Y., Li, Z., Zhang, M., Driggs-Campbell, K., Wu, J., Fei-Fei, L., and Li, Y. D³fields: Dynamic 3d descriptor fields for zero-shot generalizable robotic manipulation. In *Conference on Robot Learning (CoRL)*, 2024.
- Xiao, T., Radosavovic, I., Darrell, T., and Malik, J. Masked visual pre-training for motor control. *arXiv preprint arXiv:2203.06173*, 2022.
- Xie, A., Lee, L., Xiao, T., and Finn, C. Decomposing the generalization gap in imitation learning for visual robotic manipulation. In *International Conference on Robotics and Automation (ICRA)*, 2024.
- Xu, J. and Wang, X. Rethinking self-supervised correspondence learning: A video frame-level similarity perspective. In *International Conference on Computer Vision (ICCV)*, 2021.
- Yen-Chen, L., Florence, P., Barron, J. T., Lin, T.-Y., Rodriguez, A., and Isola, P. NeRF-Supervision: Learning dense object descriptors from neural radiance fields. In *International Conference on Robotics and Automation (ICRA)*, 2022.
- Yu, T., Quillen, D., He, Z., Julian, R., Hausman, K., Finn, C., and Levine, S. Meta-world: A benchmark and evaluation for multi-task and meta reinforcement learning. In *Conference on Robot Learning (CoRL)*, 2020.
- Zhou, J., Wei, C., Wang, H., Shen, W., Xie, C., Yuille, A., and Kong, T. ibot: Image bert pre-training with on-line tokenizer. In *International Conference on Learning Representations (ICLR)*, 2022.
- Zhou, Y., Sonawani, S., Phielipp, M., Ben Amor, H., and Stepputtis, S. Learning modular language-conditioned robot policies through attention. *Autonomous Robots*, 2023a.
- Zhou, Y., Sonawani, S., Phielipp, M., Stepputtis, S., and Amor, H. Modularity through attention: Efficient training and transfer of language-conditioned policies for robot manipulation. In *Conference on Robot Learning (CoRL)*, 2023b.

A. Evaluated PVRs

In this section we describe the PVRs evaluated in our experiments. Table A1 summarises the architecture, training objective, and pre-training dataset for each PVR, along with its highlight that motivates our evaluation.

Table A1. Summary of the PVRs evaluated in our experiments, and their respective highlights that motivate our selection. The dataset size denotes the number of images unless specified otherwise. † The number of frames extracted from videos. * The number of videos. 🤖 Pre-trained for robotics.

Model	Architecture	Training Objective	Dataset (Size)	Highlight	🤖
MAE (He et al., 2022)	ViT-B/16	Masked Image Modeling	ImageNet (1.2M)	Pioneered MIM model	✗
VC-1 (Majumdar et al., 2023)	ViT-B/16	Masked Image Modeling	Ego4D+MNI (5.6M [†])	MIM for robot learning	✓
DINOv1 (Caron et al., 2021)	ViT-B/16	Self Distillation	ImageNet (1.2M)	Seminal self distillation-based SSL model	✗
iBOT (Zhou et al., 2022)	ViT-B/16	Masked Image Modeling + Self Distillation	ImageNet (14M)	Competitive SSL model	✗
DINOv2 (Oquab et al., 2024)	ViT-B/14	Masked Image Modeling + Self Distillation	LVD (142M)	State-of-the-art SSL model	✗
ViT (Dosovitskiy et al., 2021)	ViT-B/16	Image Classification	ImageNet (14M)	Earliest Vision Transformer	✗
CLIP (Radford et al., 2021)	ViT-B/16	Vision-Language Contrastive	LAION (2B)	Widely used VLM	✗
MoCov2 (Chen et al., 2020)	ResNet-50	Contrastive	ImageNet (1.2M)	Seminal contrastive learning model	✗
DenseCL (Wang et al., 2021)	ResNet-50	Contrastive (local)	ImageNet (1.2M)	Localised SSL representation	✗
SwAV (Caron et al., 2020)	ResNet-50	Cluster Assignment Prediction	ImageNet (1.2M)	Representative cluster-based SSL model	✗
VICRegL (Bardes et al., 2022)	ResNet-50	VICReg (global and local)	ImageNet (1.2M)	SSL at both global and local levels	✗
VFS (Xu & Wang, 2021)	ResNet-50	Self Distillation (video-based)	Kinetics (240K*)	Representative video frame-based SSL model	✗
VIP (Ma et al., 2023b)	ResNet-50	Goal-conditioned Value Function Learning	Ego4D (5M [†])	Reward-oriented representation for robotics	✓
R3M (Nair et al., 2022)	ResNet-50	Time Contrastive and Language Alignment	Ego4D (5M [†])	Temporal-aware representation for robotics	✓

B. On the use of PVRs in Downstream Robotics Tasks

As discussed in Section 1, while the application of pre-trained visual representations (PVRs) in visuo-motor policy learning is still nascent, these models have proven instrumental in other downstream robotics tasks.

For instance, in manipulation tasks utilizing dense visual descriptors without a learnable policy component, the field has transitioned from training these features from scratch (Sundaresan et al., 2020; Ganapathi et al., 2021; Manuelli et al., 2021; Florence et al., 2019; 2018; Yen-Chen et al., 2022) to leveraging features extracted from vision foundation models such as DINO (Caron et al., 2021; Oquab et al., 2024) and CLIP (Radford et al., 2021). A common strategy involves integrating these features into 3D spatial representations, as exemplified by works like F3RM (Shen et al., 2023), D³Fields (Wang et al., 2024), and Click2Grasp (Tsagkas et al., 2024). Similarly, PVRs have significantly contributed to semantic mapping, particularly when incorporating language components, as demonstrated in VL-Fields (Tsagkas et al., 2023) and CLIP-Fields (Shafullah et al., 2023).

However, PVRs have yet to gain traction in robot learning frameworks. The foundational study by (Chi et al., 2023) shows that diffusion policies conditioned on R3M (Nair et al., 2022) features perform worse than those conditioned on visual encoders trained end-to-end. Notably, policies trained with PVRs tend to produce jittery actions and are prone to getting stuck, which may be linked to an incorrect assumption of the Markov property. Consequently, end-to-end training of visual encoders alongside the policy remains the preferred approach (e.g., (Sochopoulos et al., 2024; Florence et al., 2021)).

Finally, an interesting side that is out of the scope of this research concerns the use of other modalities in robot learning. More specifically, a group of recent works has shifted from PVRs that utilise only image data but also language (Li et al., 2023; Gupta et al., 2024; Ma et al., 2023a; Karamcheti et al., 2023).

C. Temporal Encoding

Figs. A1 and A2 extend the methodology from Fig. 1 to real-world data from (Chi et al., 2023; Zhou et al., 2023a;b). As shown, similar issues arise, such as the temporal entanglement of features. While testing our approach on a real robot remains part of our future work, these results provide evidence that the challenges identified in simulation persist in real-world scenarios. Although it is well established that simulations like MetaWorld serve as a reliable proxy for real-world performance (Silwal et al., 2024), these figures underscore the significance of our findings and the necessity of our proposed solutions.

C.1. On the quality of simulation data

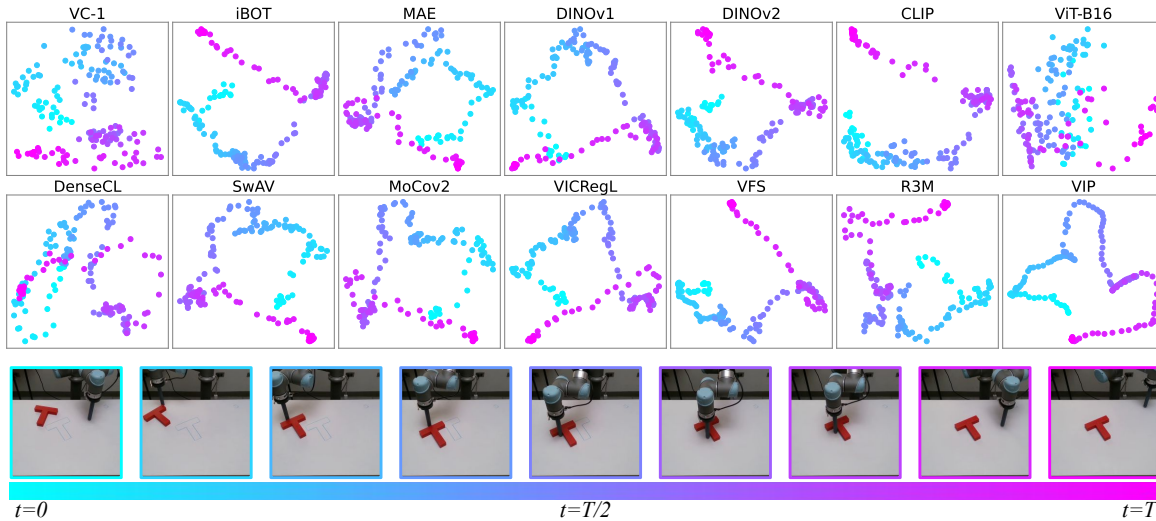


Figure A1. Visualisation of PCA results for the features extracted from frames of an expert demonstration trajectory from **the real-world** in the Push-T task (Chi et al., 2023) across the studied PVRs. In this example, we see mostly a cluster forming when the robot has pushed the T block to its outline and makes very small adjustments.

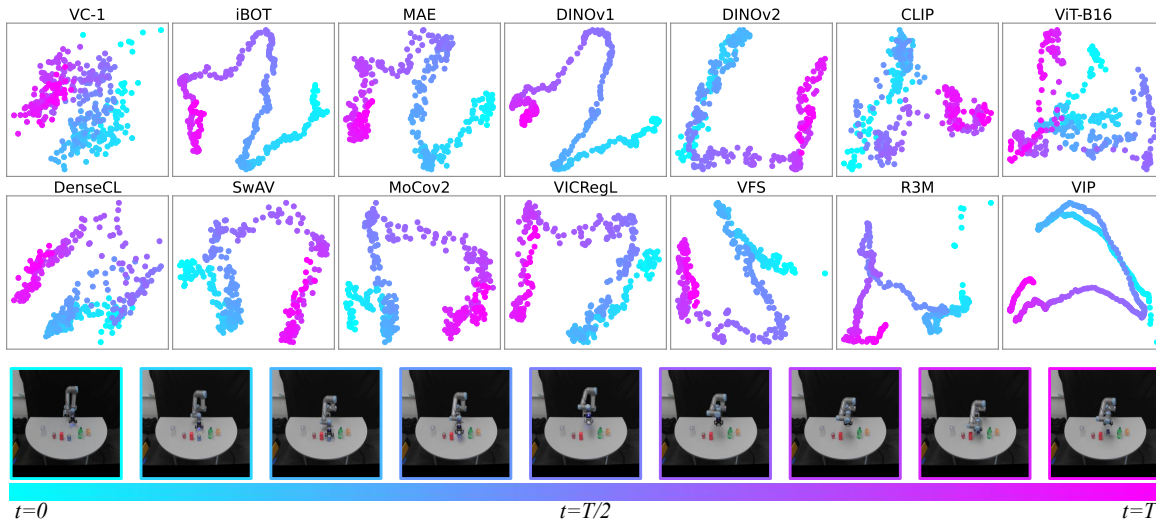


Figure A2. Visualisation of PCA results for the features extracted from frames of an expert demonstration trajectory from **the real-world** in the ASU Table (Zhou et al., 2023a;b) task across the studied PVRs. In this example, entanglement occurs mostly from the fact that the robot picks up the can, rotates it by 90 degrees and then places it in the exact same spot.

C.2. TE Per Task Results

In Table A2, we provide the IQM success rate of policies trained with each PVR-task pair, using the raw features extracted from the PVR, the features temporally augmented with the FLARE method and finally, the features temporally augmented with TE (ours). The results indicate that incorporating TE significantly improves performance compared to using no temporal information. This is supported by both the Wilcoxon test ($p < 10^{-30}$) and paired t-test ($p < 10^{-26}$). The data is not normally distributed. Additionally, TE also outperforms FLARE, with statistically significant differences observed in both the Wilcoxon test ($p \approx 4.38 \times 10^{-5}$) and paired t-test ($p \approx 1.47 \times 10^{-4}$).

Table A2. Evaluation of trained policies across 10 tasks, utilising features from 14 different PVRs. Results are reported without any temporal augmentation (T: -), with the FLARE method (T: ∇) and with TE of the timestep (T: ◇). We mark with green the temporal encoding results that outperformed the other two methods. Similarly, with red for the no augmentation case and yellow for FLARE.

	T	DINOv2	DINOv1	MAE	CLIP	ViT	iBot	VC1	MoCov2	SWAV	VIP	DenseCL	R3M	VFS	VICRegL
Bin Picking	-	43.3 ± 0.5	33.3 ± 2.4	50.0 ± 4.3	56.3 ± 1.9	26.7 ± 5.2	41.7 ± 3.3	52.0 ± 2.9	56.7 ± 7.4	54.3 ± 3.3	32.7 ± 3.3	40.7 ± 3.4	40.3 ± 5.4	51.0 ± 4.1	46.0 ± 7.8
	∇	28.3 ± 3.1	35.3 ± 2.4	18.7 ± 2.1	46.7 ± 4.8	32.7 ± 5.2	22.0 ± 2.2	45.0 ± 4.9	38.3 ± 9.6	42.3 ± 0.5	37.7 ± 7.1	29.7 ± 1.7	49.7 ± 6.5	62.3 ± 3.1	44.7 ± 10.4
	◇	66.3 ± 5.2	53.7 ± 3.4	53.7 ± 0.9	71.0 ± 2.2	56.0 ± 2.4	53.3 ± 4.9	53.7 ± 9.9	65.7 ± 3.8	63.7 ± 4.6	51.7 ± 2.1	40.0 ± 8.0	77.0 ± 6.7	79.7 ± 0.9	68.7 ± 0.5
Disassemble	-	85.7 ± 0.5	77.3 ± 0.5	35.7 ± 1.9	76.7 ± 4.2	81.0 ± 2.2	90.3 ± 3.1	74.7 ± 2.9	92.3 ± 1.2	91.3 ± 0.5	85.3 ± 2.5	87.3 ± 2.9	83.0 ± 3.6	80.0 ± 1.6	89.0 ± 0.8
	∇	91.7 ± 1.7	88.7 ± 4.0	76.7 ± 2.5	72.7 ± 3.4	82.0 ± 1.4	89.0 ± 2.4	84.7 ± 3.7	91.3 ± 0.5	91.0 ± 2.2	24.0 ± 7.3	87.3 ± 1.7	91.3 ± 3.9	92.0 ± 0.8	89.7 ± 2.5
	◇	93.7 ± 0.9	91.0 ± 1.6	92.0 ± 2.2	83.3 ± 2.9	90.7 ± 1.7	95.3 ± 2.1	77.3 ± 0.5	92.0 ± 0.8	94.3 ± 0.9	91.0 ± 2.2	90.0 ± 0.8	91.0 ± 2.9	93.7 ± 2.5	93.0 ± 1.6
Coffee Pull	-	46.0 ± 3.6	53.3 ± 2.1	42.3 ± 3.3	42.0 ± 0.8	49.3 ± 1.2	55.7 ± 0.5	19.3 ± 7.1	72.3 ± 1.9	72.0 ± 0.8	99.7 ± 0.5	62.3 ± 1.7	89.0 ± 2.4	89.3 ± 3.8	82.7 ± 5.0
	∇	47.3 ± 5.4	50.7 ± 1.7	63.0 ± 5.0	50.3 ± 2.1	49.0 ± 1.6	57.0 ± 1.6	60.3 ± 4.2	77.0 ± 0.8	77.0 ± 2.2	88.3 ± 1.7	59.3 ± 0.5	99.0 ± 0.8	86.3 ± 3.3	74.0 ± 2.2
	◇	56.0 ± 3.3	54.0 ± 2.4	47.7 ± 4.7	51.3 ± 3.3	45.0 ± 1.4	58.0 ± 2.9	61.0 ± 3.7	72.0 ± 2.4	77.0 ± 3.6	99.0 ± 0.8	63.0 ± 3.7	93.7 ± 2.6	92.7 ± 2.6	79.3 ± 2.5
Shelf Place	-	9.0 ± 4.2	6.0 ± 2.2	5.0 ± 0.8	10.3 ± 0.9	1.3 ± 1.9	4.0 ± 0.0	2.7 ± 1.7	17.0 ± 4.5	28.7 ± 1.2	28.7 ± 4.5	8.0 ± 0.8	39.7 ± 4.8	20.3 ± 3.3	20.7 ± 4.2
	∇	8.0 ± 0.8	6.7 ± 3.1	8.7 ± 1.2	9.3 ± 0.5	4.3 ± 1.9	3.7 ± 1.9	1.7 ± 0.5	22.7 ± 1.7	23.3 ± 3.4	32.0 ± 1.6	15.0 ± 4.2	43.7 ± 3.4	21.0 ± 1.6	27.7 ± 2.6
	◇	3.7 ± 2.1	5.0 ± 1.4	4.7 ± 2.9	12.3 ± 1.7	6.7 ± 2.5	4.0 ± 0.8	4.3 ± 2.1	20.7 ± 4.2	33.7 ± 5.2	22.0 ± 2.9	12.3 ± 2.1	33.3 ± 1.2	26.7 ± 2.9	28.0 ± 0.8
Peg Insert Side	-	30.7 ± 1.2	23.7 ± 2.1	23.0 ± 1.4	18.7 ± 3.7	4.3 ± 1.2	20.7 ± 3.4	22.0 ± 1.4	34.0 ± 0.8	48.3 ± 3.4	34.0 ± 2.2	32.3 ± 3.7	59.7 ± 0.5	38.0 ± 5.7	38.7 ± 2.1
	∇	24.3 ± 3.8	33.0 ± 5.4	28.3 ± 4.7	13.7 ± 4.9	12.0 ± 2.8	25.3 ± 1.7	17.0 ± 2.4	35.7 ± 3.7	39.3 ± 6.6	44.7 ± 6.3	23.3 ± 2.4	34.7 ± 5.2	35.7 ± 0.9	43.7 ± 3.4
	◇	30.7 ± 0.9	31.3 ± 2.4	27.3 ± 2.9	18.3 ± 0.5	25.7 ± 1.7	11.0 ± 2.8	8.7 ± 0.5	50.7 ± 0.5	37.3 ± 1.7	74.0 ± 0.8	40.3 ± 3.3	69.0 ± 0.8	50.3 ± 3.4	44.3 ± 3.4
Box Close	-	44.0 ± 2.2	59.3 ± 5.4	63.0 ± 6.7	46.3 ± 5.4	57.7 ± 7.4	61.7 ± 1.7	56.3 ± 6.1	56.3 ± 5.3	53.0 ± 2.2	48.7 ± 6.2	59.7 ± 4.5	49.0 ± 6.2	57.3 ± 1.2	61.3 ± 4.5
	∇	45.0 ± 0.8	61.0 ± 1.6	64.0 ± 7.8	55.0 ± 1.6	54.0 ± 2.2	64.7 ± 5.6	60.3 ± 2.1	58.7 ± 5.4	57.7 ± 4.8	33.3 ± 18.8	57.3 ± 5.3	41.3 ± 2.6	62.0 ± 1.6	67.3 ± 2.5
	◇	56.7 ± 1.2	68.3 ± 0.5	57.0 ± 2.2	63.3 ± 5.0	73.3 ± 1.7	61.0 ± 5.0	71.0 ± 2.2	67.0 ± 5.0	61.0 ± 0.8	52.7 ± 0.5	62.3 ± 3.7	68.0 ± 2.2	72.0 ± 3.7	68.3 ± 3.3
Assembly	-	67.3 ± 3.7	61.7 ± 2.9	7.3 ± 0.9	35.3 ± 2.5	55.7 ± 2.5	72.7 ± 3.8	82.3 ± 0.5	90.3 ± 3.1	94.3 ± 0.5	5.0 ± 3.6	97.0 ± 2.2	93.3 ± 1.2	92.3 ± 1.7	93.0 ± 2.4
	∇	24.7 ± 0.5	47.3 ± 2.9	59.7 ± 2.1	34.3 ± 2.5	39.7 ± 3.8	63.3 ± 0.9	50.3 ± 2.1	82.3 ± 4.7	93.0 ± 2.2	35.7 ± 29.8	77.0 ± 2.9	98.3 ± 2.4	92.7 ± 2.1	93.3 ± 1.2
	◇	73.0 ± 4.1	79.3 ± 3.1	66.0 ± 4.3	53.7 ± 1.9	79.3 ± 2.1	61.3 ± 2.5	63.3 ± 3.1	90.3 ± 4.5	91.0 ± 2.8	71.7 ± 8.7	93.7 ± 3.4	100.0 ± 0.0	87.7 ± 3.3	92.7 ± 2.9
Button Press Wall	-	70.3 ± 4.5	76.0 ± 2.9	49.3 ± 1.9	76.7 ± 4.2	62.3 ± 9.0	57.7 ± 1.2	31.0 ± 0.0	57.3 ± 0.9	69.3 ± 2.6	22.3 ± 17.4	52.0 ± 7.9	63.3 ± 3.9	58.7 ± 4.6	51.3 ± 5.4
	∇	59.3 ± 7.0	84.7 ± 2.9	63.3 ± 4.9	67.7 ± 1.2	64.7 ± 1.2	74.0 ± 5.4	65.0 ± 0.8	63.3 ± 7.5	64.0 ± 4.9	65.7 ± 14.8	68.0 ± 2.9	60.3 ± 2.6	62.0 ± 6.5	50.0 ± 1.6
	◇	79.0 ± 4.2	77.3 ± 2.4	85.0 ± 0.0	82.0 ± 2.8	69.0 ± 4.3	74.3 ± 0.9	63.0 ± 3.7	77.7 ± 8.7	64.7 ± 3.4	6.3 ± 2.5	83.3 ± 4.8	54.7 ± 1.2	58.0 ± 5.7	67.0 ± 12.7
Pick Place Wall	-	39.7 ± 7.4	29.3 ± 4.5	41.0 ± 4.5	36.0 ± 5.7	59.3 ± 7.3	25.7 ± 1.7	49.7 ± 7.1	84.0 ± 1.6	69.3 ± 1.7	54.0 ± 15.7	61.7 ± 5.4	67.0 ± 4.9	80.7 ± 0.5	76.3 ± 2.4
	∇	47.0 ± 6.2	69.3 ± 5.3	52.0 ± 4.2	49.0 ± 2.2	64.3 ± 3.3	58.7 ± 2.1	44.3 ± 2.6	88.7 ± 2.4	89.0 ± 0.8	86.3 ± 2.5	59.0 ± 9.6	95.3 ± 0.5	90.0 ± 0.8	95.0 ± 2.4
	◇	24.7 ± 2.5	59.0 ± 7.3	26.7 ± 4.5	29.7 ± 4.2	40.0 ± 2.2	24.3 ± 0.9	26.0 ± 4.3	79.7 ± 0.9	62.0 ± 3.7	86.7 ± 2.6	49.7 ± 2.6	66.0 ± 0.8	83.3 ± 5.2	73.3 ± 4.6
Drawer Open	-	90.7 ± 1.2	92.0 ± 0.0	92.7 ± 1.2	87.7 ± 0.9	89.3 ± 0.5	96.3 ± 1.2	95.7 ± 1.7	93.3 ± 1.9	93.3 ± 1.9	95.7 ± 1.7	100.0 ± 0.0	90.3 ± 1.2	95.0 ± 0.8	92.0 ± 0.0
	∇	93.0 ± 1.4	93.3 ± 1.9	94.0 ± 1.6	90.3 ± 1.2	89.3 ± 0.5	99.7 ± 0.5	100.0 ± 0.0	95.0 ± 0.8	91.7 ± 0.5	99.3 ± 0.9	100.0 ± 0.0	100.0 ± 0.0	95.0 ± 0.8	92.0 ± 0.0
	◇	100.0 ± 0.0	100.0 ± 0.0	100.0 ± 0.0	99.3 ± 0.9	99.3 ± 0.9	100.0 ± 0.0	100.0 ± 0.0	95.7 ± 0.5	100.0 ± 0.0	95.7 ± 1.7	98.0 ± 0.8	100.0 ± 0.0	100.0 ± 0.0	94.7 ± 0.9

C.3. Tuning Temporal Encoding Hyperparameters

We fine-tune TE’s scale and dimensionality using 4 PVRs (MAE, DINOv1, SwAV, R3M) and 4 MetaWorld tasks (Bin Picking, Coffee Pull, Disassemble, Pick and Place). Table C.3 shows the percentage of PVR-task pairs benefiting from TE across different hyperparameters, with $D = 64, s = 100$ yielding the most improvements. As seen in Table C.3, this setting also achieves one of the highest average performance gains.

Dims	10	100	1000
64	56.25%	84.38%	75.00%
128	81.25%	75.00%	75.00%
256	75.00%	81.25%	81.25%

Table A3. Percentage of PVR-Task pairs were TE led to performance increase.

Dims	10	100	1000
64	11.26 ± 6.66	11.82 ± 5.72	9.08 ± 4.43
128	8.51 ± 7.61	11.97 ± 4.79	11.03 ± 5.39
256	8.89 ± 4.84	11.38 ± 6.17	11.82 ± 6.73

Table A4. Average boost (i.e., for the PVR-Task pairs that benefited from TE) values for each scale and dimension combination.

C.4. MetaWorld Temporal Variability of Expert Demos

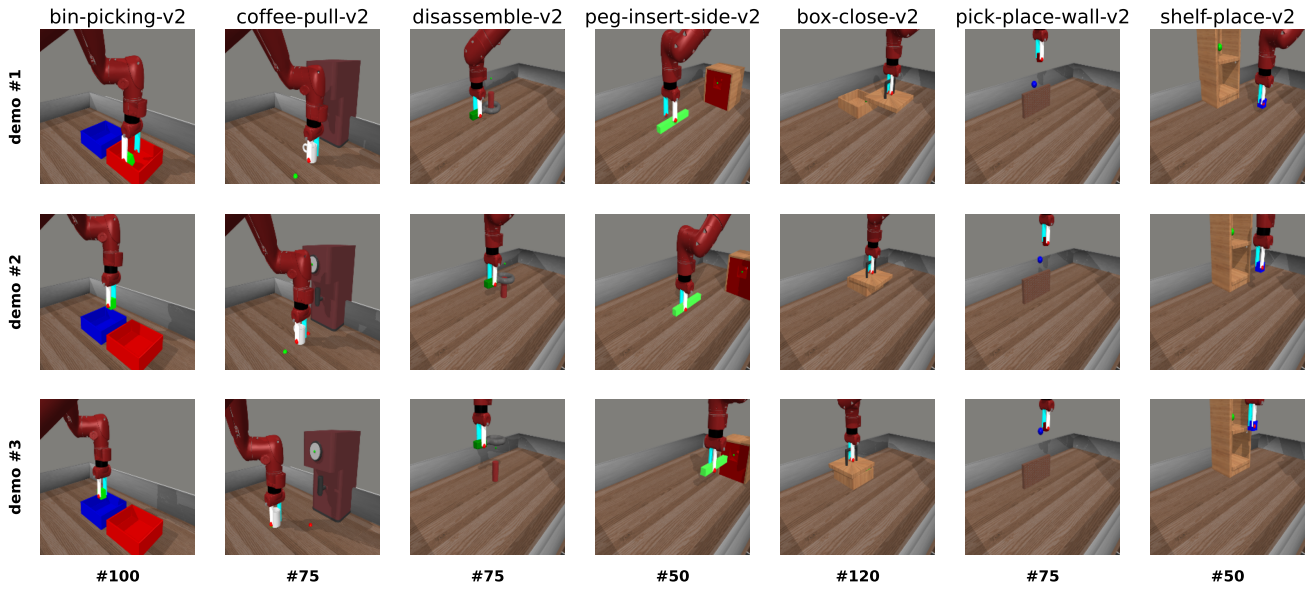


Figure A3. Illustration of temporal variability in Metaworld expert demonstrations. Each column represents a different task, with each row showing a frame captured at the same time-step across three separate demonstrations. The lack of perfect synchronisation between demonstrations highlights variability in task progression.

D. Attentive Feature Aggregation

D.1. AFA Per Task Results

In Fig. A4 we provided the results for each PVR+AFA+TE-task pair, for both in-domain scenes and visually altered scenes.

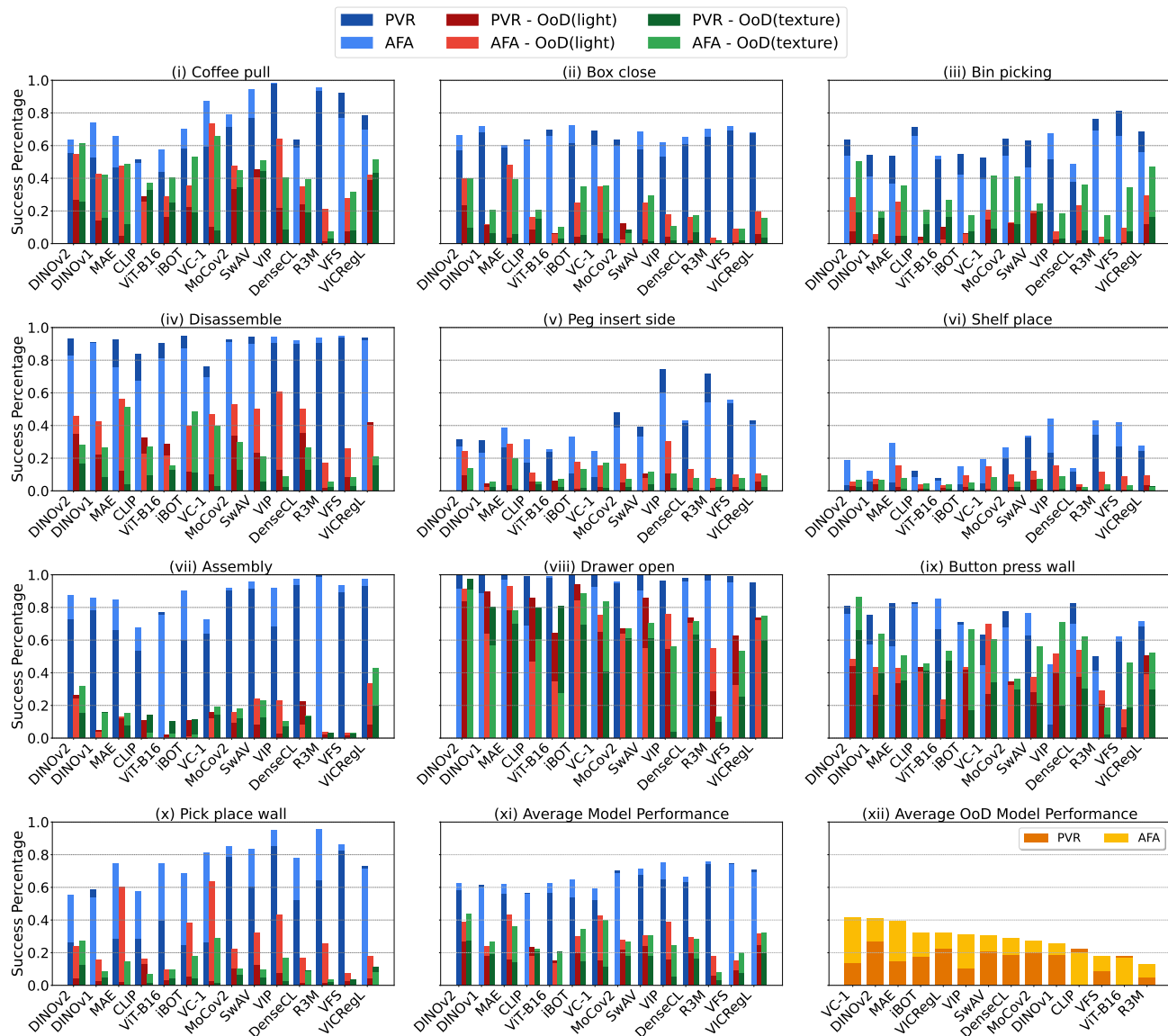


Figure A4. Evaluation of the AFA module in both in-domain and out-of-domain scenarios, including tabletop texture and lighting perturbations. Sub-figures (i)-(x) illustrate policy performance for individual tasks. Sub-figure (xi) presents the average performance across all tasks, while sub-figure (xii) displays the average OOD performance, with PVRs sorted by descending ABC performance.

D.2. Scene Perturbations

To test the robustness of trained policies we visualise modify the scenes in the evaluation either by changing the lighting or by randomly changing the tabletop texture. Note that all policies are evaluated in the same perturbations for fairness.

Randomizing the scene’s lighting properties: The brightness of the scene is altered by adjusting the diffuse light

components, where each colour channel (red, green, blue) is randomly set to a value between 0.3 and 1.0. The specular highlights are similarly randomized, with lower intensity values ranging from 0.1 to 0.5. Additionally, the position of each light source is varied randomly within a 3D space, spanning horizontal and vertical shifts between -2 and 2 units and height adjustments between 0.5 and 3 units. Lastly, the direction of the lights is randomized, allowing for changes in their angular orientation, with each directional component varying between -1 and 1 for horizontal/vertical angles and up to -1 for downward angles.

Randomizing the Tabletop’s texture: In Fig. A5 we provide the textures that we utilised in our experiments, some of which are borrowed from (Xie et al., 2024). Some are visually similar to the texture used in the training demos and others are vibrant, with patterns that hold semantic information that could potentially attract the attention of a PVR. Nevertheless, by observing the evaluation rollouts, policies can fail and succeed in both out-of-distribution cases.

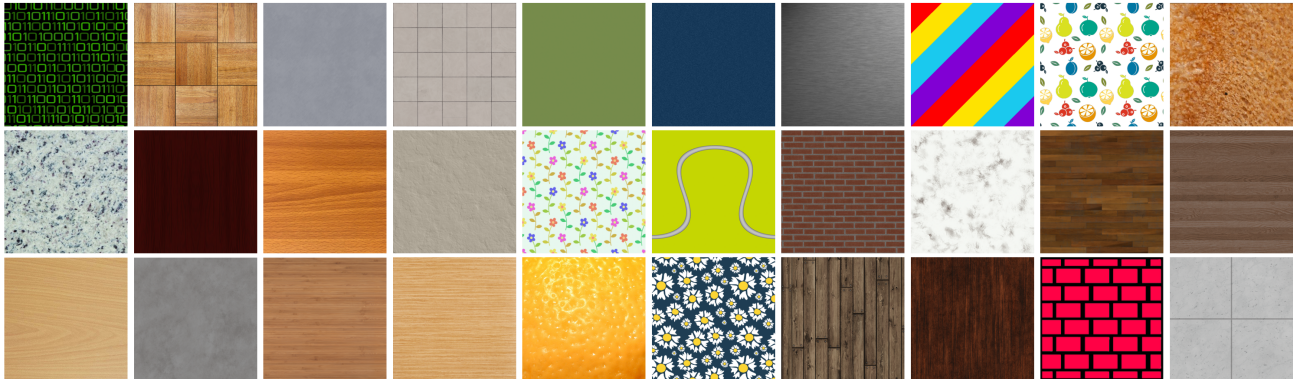


Figure A5. Visualisation of the different table textures used in the evaluations of Section 4.3. The additional textures that are not provided by MetaWorld were borrowed from (Xie et al., 2024).

D.3. Ablation: Does AFA’s success stem from its increased capacity?

Does AFA’s success stem from its increased capacity? We make the policy network deeper (*i.e.*, from 594,956 to 1,645,580) to roughly match the number of trainable parameters of the AFA (*i.e.*, 1,774,336) by adding more layers. In Fig. A6 we visualise the results both in and out of domain for policies trained with AFA and with the deeper MLP. As is evident, AFA still has the better robustness performance.

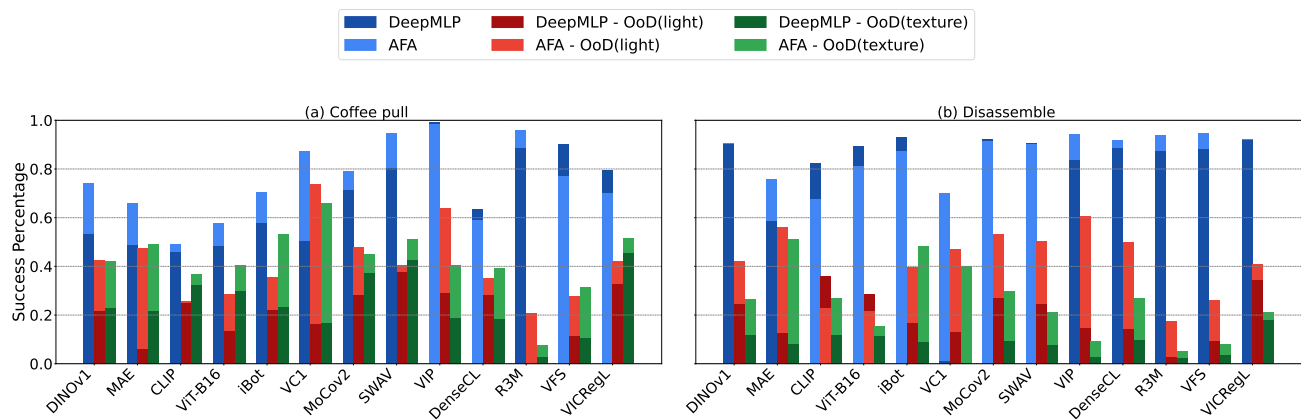


Figure A6. Results from policies trained with either AFA or with a deeper MLP of capacity comparable to that of AFA.

D.4. Qualitatively explaining AFA’s performance boost

In Fig. A7, we present additional comparisons between the attention heatmaps of the PVRs and their corresponding trained AFAs. These visualizations illustrate how the CLS token attends to different patches compared to the trained query token, offering a general sense of what the models prioritise. While this does not imply that trained AFAs are entirely robust to visual changes in the scene (*e.g.*, note that iBOT+AFA still allocates some attention to patches containing the robot’s cast shadow), we observe a consistent trend: the attention heatmaps become more focused, particularly on regions relevant to the task.

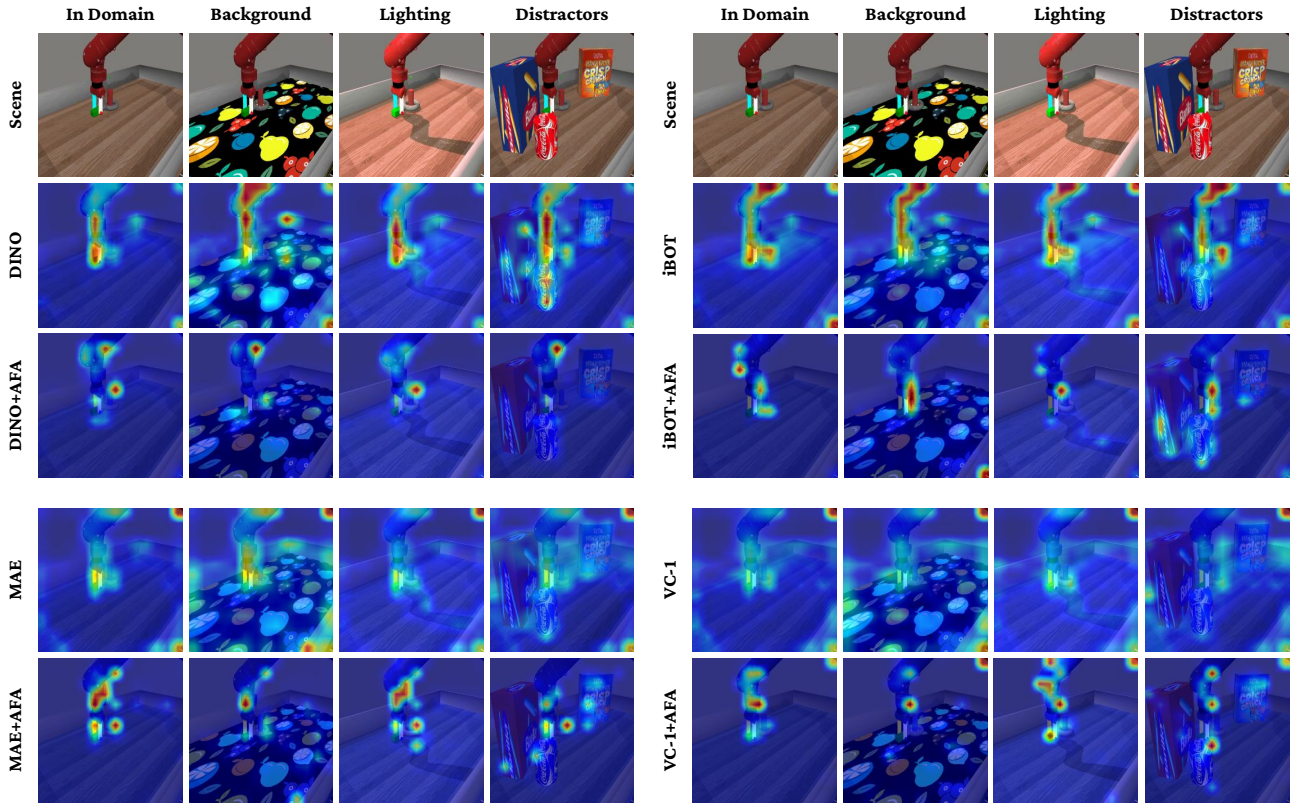


Figure A7. Additional comparisons between PVR and PVR+AFA attention heatmaps.